J. Cent. South Univ. (2021) 28: 1724−1736
DOI: https://doi.org/10.1007/s11771-021-4729-3

Springer

Stress-strain-acoustic responses in failure process of coal rock with different height to diameter ratios under uniaxial compression

GUO Yu-xia(郭育霞)[1, 2], ZHAO Yong-hui(赵永辉)[1, 2], WANG Sheng-wei(王胜伟)[1, 2], FENG Guo-rui(冯国瑞)[1, 2], ZHANG Yu-jiang(张玉江)[1, 2], RAN Hong-yu(冉洪宇)[1, 2]

1. College of Mining Engineering, Taiyuan University of Technology, Taiyuan 030024, China;
2. Shanxi Province Research Centre of Green Mining Engineering Technology, Taiyuan 030024, China

Abstract: Residual coal pillars play an important role in mining the adjacent coal seam safely, managing the gobs and maintaining the stability of abandoned coal mines. The height to diameter ratio (*H*/*D*) affects the stability of residual coal pillars. In this study, uniaxial compressive tests of coal specimens with five *H*/*D* (2.0, 1.5, 1.0, 0.8 and 0.6) were performed, and the stress, strain and acoustic emission (AE) were monitored. Results show that the uniaxial compressive strength (UCS) and peak strain increase with *H*/*D* decreasing. An empirical equation is proposed to calculate the UCS based on the *H*/*D*. The AE activities during coal failure process can be separated into four periods. The span of quiet period and rapid decline period shorten with *H*/*D* decreasing. The smaller the *H*/*D* is, the more complicated the failure characteristics of coal will be. The failure form of coal with *H*/*D* of 2.0, 1.5, and 1.0 is primarily shear failure, while splitting failure along the axial direction is the mainly mode when *H*/*D* is 0.8 or 0.6. The initiation, expansion, aggregation and connection of micro-cracks can be reflected by the real-time spatial evolution of AE event points.

Key words: residual coal pillar; height to diameter ratio; uniaxial compression; acoustic emission; micro-crack evolution

Cite this article as: GUO Yu-xia, ZHAO Yong-hui, WANG Sheng-wei, FENG Guo-rui, ZHANG Yu-jiang, RAN Hong-yu. Stress-strain-acoustic responses in failure process of coal rock with different height to diameter ratios under uniaxial compression [J]. Journal of Central South University, 2021, 28(6): 1724−1736. DOI: https://doi.org/10.1007/s11771-021-4729-3.

1 Introduction

As an important raw material for electric power generation and chemical production, coal resource has greatly promoted the industrial and economic development of the world. In recent years, due to exhausted recoverable reserves, low coal prices, high underground mining cost and geological challenges, a large amount of coal mine was abandoned in many coal-producing countries [1−4]. In these abandoned coal mines, many residual coal pillars with different height *H* to diameter *D* ratios have been arranged for supporting the overburden strata and maintaining the stability of the roadways and working faces [5, 6]. These factors not only reduce the recovery rate of coal resources, but also bring many difficulties to manage the gobs, such as pillar failure, roof collapse and surface subsidence [7−10]. Understanding the influence of *H*/*D* on the residual coal pillars' performance can help to predict the failure of the residual coal pillars and maintain the stability of

Foundation item: Projects(51974192, 52004172) supported by the National Natural Science Foundation of China; Project(51925402) supported by the Distinguished Youth Funds of National Natural Science Foundation of China; Project(U1710258) supported by the Joint Funds of National Natural Science Foundation of China and Shanxi Province, China
Received date: 2021-02-23; **Accepted date:** 2021-04-13
Corresponding author: FENG Guo-rui, PhD, Professor; Tel: +86-13643697785; E-mail: fguorui@163.com; ORCID: https://orcid.org/0000-0003-0939-4248; ZHANG Yu-jiang, PhD, Associate Professor; Tel: +86-18636157047; E-mail: ylczyj@yeah.net; ORCID: https://orcid.org/0000-0001-8626-5680

abandoned coal mines.

Many scholars have devoted a great deal effort to investigate the effects of size on the performance of coal and rocks. DAS [11] and OZKAN et al [12] performed uniaxial compression tests on rock specimens with different *H*/*D*s, and presented that *H*/*D* has an important influence on the failure property of rock. QI et al [13] studied the size effect on the dynamic strength of rock mass. HE et al [14] investigated the relationship between the *H*/*D* and uniaxial compressive strength (UCS) of gypsum sample, and found that the UCS, residual strength and elastic modulus increase with the *H*/*D* decreasing. STAVROU et al [15] proposed the relationship between rock strength and rock size and in-situ conditions. Some scholars have used various numerical simulation software to analyze the influence of size on rock strength [16−18].

The above research is based on macroscopic mechanical tests. Scholars also have used various observation techniques to study the strength and microcrack evolution characteristics of rock and concrete, such as X-ray computed tomography (CT) [19], ultrasonic testing [20], resistivity testing [21, 22], scanning electron microscopy (SEM) [23−26], digital image correlation (DIC) [27−29], electromagnetic radiation (EMR) [30] and acoustic emission (AE) [31−36]. Among these microscopic observation techniques, AE technology is widely used as a particularly useful method to study crack propagation characteristics and provide early warning signals for rock specimens and engineering structural instability due to its high sensitivity to micro-cracks.

Previous studies offered good insight to the mechanical properties and AE parameter characteristics of concrete and rock at loading process. However, the existing researches seldom study the relationship between the mechanical properties and internal crack evolution about the residual coal pillars with different *H*/*D*s. The uniaxial compression tests were performed using coal or rock specimens (*H*/*D* was 2.0) to study their AE characteristics during loading process [37, 38]. In this study, the coal specimens which were taken from the residual coal pillars in Jinhuagong Coal Mine were used to specifically investigate the mechanical properties of residual coal pillars with different *H*/*D*s. The AE counts, the cumulative AE counts, and the spatial distribution of AE events of coal specimens under uniaxial compression also were monitored to analyze the influence of *H*/*D* on the fracturing process.

2 Experimental methodology

2.1 Coal specimens

The coal specimens were taken from massive coals which were excavated from the No. 6 coal seam in Jinhuagong Coal Mine, Shanxi Province, China. The diameter of the coal specimens was 50 mm, and the height was 30, 40, 50, 75 and 100 mm (the *H*/*D* of coal specimen was 0.6, 0.8, 1.0, 1.5 and 2.0, respectively).

In order to meet the standard of the International Society of Rock Mechanics [39] and ensure the reliability of the experimental results, the coal specimens were cored along the same orientation of the massive coals. The cores were cut and polished to ensure the non-parallelism of the upper and lower end faces no more than ± 0.3 mm, and the deviation of the two end faces from the axis of coal specimen no more than ±0.25°. It is noticed that there is no visible crack and damage on the surface of specimens selected for the test. To ensure that there is no internal crack in the specimens, the KON-NM-4B non-metal ultrasonic testing instrument was used to conduct P-wave tests on these coal specimens, and four specimens which had a relatively concentrated P-wave velocity of each *H*/*D* were selected as a group [40].

After the preparation of the experimental coal specimens, a series of tests were conducted to obtain their physical and mechanical parameters. The specific parameters of the coal specimens are shown in Table 1.

2.2 Experimental apparatus

The experimental system mainly includes the loading system and the AE monitoring system. The loading system is composed of WAW1000 electro-hydraulic servo-control universal testing machine. The maximum loading capacity was 1000 kN, and its loading measurement resolution was 0.005‰. The displacement-controlled loading mode with a rate of 0.002 mm/s was adopted to perform the uniaxial compressive tests in this study.

The AE monitoring system mainly consisted of RS-2A AE piezoceramic sensor, AE pre-amplifiers,

Table 1 Physical and mechanical parameters of coal specimens

Group	No.	Height/mm	Diameter/mm	*H*/*D*	Mass/g	Density/(kg·m^{-3})	UCS/MPa	Average UCS/MPa
1	1-1	100.02	48.94	2.04	238.15	1265.74	21.36	22.31
	1-2	100.90	48.74	2.07	239.69	1273.20	22.84	
	1-3	100.04	49.02	2.04	239.86	1270.42	23.12	
	1-4	100.16	48.90	2.05	238.03	1265.41	21.93	
2	2-1	75.90	48.92	1.55	180.52	1265.38	26.28	24.96
	2-2	75.70	49.08	1.54	180.93	1263.33	24.64	
	2-3	75.70	49.10	1.54	179.54	1252.60	23.55	
	2-4	75.30	48.94	1.54	178.04	1256.91	25.36	
3	3-1	49.90	49.04	1.02	117.49	1246.55	29.15	28.80
	3-2	50.40	49.06	1.03	119.28	1251.96	28.34	
	3-3	50.58	48.90	1.03	118.70	1249.58	28.07	
	3-4	50.86	49.10	1.04	120.06	1246.72	29.65	
4	4-1	40.94	49.04	0.83	96.47	1247.54	30.12	30.46
	4-2	39.14	49.06	0.80	92.42	1249.11	29.70	
	4-3	39.88	49.10	0.81	94.64	1253.33	32.04	
	4-4	39.10	49.08	0.80	92.33	1248.15	29.97	
5	5-1	30.32	49.12	0.62	72.59	1263.40	43.20	42.96
	5-2	30.28	49.12	0.62	71.75	1250.43	42.42	
	5-3	30.26	49.06	0.62	72.41	1265.86	43.54	
	5-4	49.14	30.30	0.62	71.66	1247.02	42.68	

AE automatic data acquisition system and AE data analysis computer. AE sensors' diameter and resonance frequency range were 18 mm and 100−400 kHz, respectively. In order to cover the volume of specimen well, the AE sensors No. 1 and No. 2, No. 3 and No. 4 were respectively treated as a group and installed symmetrically on a same plane and was fixed by adhesive tapes, and the two groups were layout orthogonally (as shown in Figure 1). The distance from the location of AE sensor No. 1 and No. 2 (or No. 3 and No. 4) to the lower (or upper) end surface of coal specimen was represented by h_l (or h_u). When the *H*/*D* of coal specimen is 2.0, 1.5 and 1.0, the h_l and h_u was 19 mm, and when the *H*/*D* is 0.8 and 0.6, the h_l and h_u was 9 mm. To obtain a satisfactory acoustic coupling effect, a thin layer of Vaseline was daubed at the interface between AE sensor and the circumferential surface of coal specimen [6, 37]. The AE pre-amplifiers were calibrated and their values were set at 40 dB. The automatic data acquisition frequency was set at 2.5 MHz.

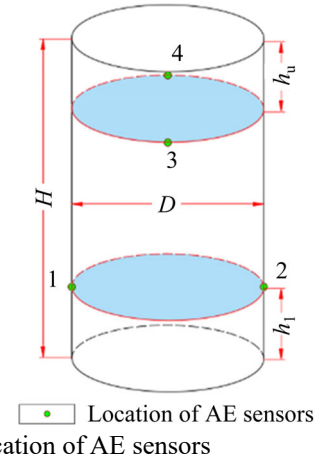

Figure 1 Location of AE sensors

2.3 Experimental procedures

Experimental equipment was calibrated and set before the uniaxial compression tests. The prepared specimens were put on the lower loading plate and then connect the relevant equipment of the two experimental systems, respectively. The upper loading plate was moved tardily downwards to slightly touch the upper end surface of the specimens. The uniaxial loading system and AE monitoring system were turned on synchronously to obtain the stress, strain and AE parameters during loading process. Loading stopped automatically when coal

specimen was overall failure, and the AE monitoring and loading system were turned off synchronously.

3 Results and discussions

The experimental results of coal samples with different *H*/*D*s (2.0, 1.5, 1.0, 0.8 and 0.6) are given in Table 1.

3.1 Mechanical characteristics

3.1.1 UCS of specimens with different *H*/*D*s

The change of specimen strength with *H*/*D* is shown in Figure 2. It can be seen that the UCS decreases gradually with the increases of the *H*/*D*, and finally approaches to a threshold value, which means that the slope of the fitting curve decreases with the increase of *H*/*D*, and approaches to 0 eventually. The UCS of specimens changes exponentially with the increase of *H*/*D*. So, Eq. (1) can be used to express the relationship between the UCS and the *H*/*D* of the coal specimens.

$$\mathrm{UCS}_{H/D}=\mathrm{UCS}_{\mathrm{M}}+\alpha\exp(\beta H/D) \quad (1)$$

where $\mathrm{UCS}_{H/D}$ is the uniaxial compressive strength of the specimens when the *H*/*D* is any value; $\mathrm{UCS}_{\mathrm{M}}$ is the UCS when $H/D\to\infty$; α and β are parameters which can be obtained by a series of uniaxial compressive tests on coal specimens with different *H*/*D*. Based on the fitting results, the parameter $\mathrm{UCS}_{\mathrm{M}}$, α and β are 23.57 MPa, 223.77 and −0.24, respectively. The correlation coefficient (R^2) is 0.965, which means that this empirical formula has a satisfactory fitting effect. The experimental data of the gypsum specimens [14] and red sandstone specimens [41] also are used to verify the applicability of Eq. (1) on different types of rocks. The results show that the parameter $\mathrm{UCS}_{\mathrm{M}}$, α and β of the gypsum specimens and red sandstone specimens are 26.86 MPa, 109.22, −0.36, and 40.32 MPa, 179.28, −0.52, respectively. The correlation coefficient (R^2) respectively is 0.928 and 0.992, which reveals that Eq. (1) fits well with the experimental data of different rock types.

3.1.2 Stress−strain curves of coal specimens with different *H*/*D*s

Figure 3 shows the axial stress−strain curves of specimens with different *H*/*D*s under uniaxial compression. The axial stress−strain curves of coal specimens with different *H*/*D*s have a similar trend as a whole. The pre-peak stage consists of micro-cracks compaction stage, elastic deformation stage and micro-cracks development stage, and as soon as the axial stress reaches the peak, the axial stress drops rapidly (post-peak failure stage). The peak stress and peak strain of specimens increase with the decrease of *H*/*D*. The values of peak stress and peak strain for specimens with *H*/*D* of 2.0, 1.5, 1.0, 0.8 and 0.6 are 21.93, 25.36, 29.65, 29.97, 43.20 MPa and 1.9×10^{-2}, 2.6×10^{-2}, 3.5×10^{-2}, 4.2×10^{-2}, 5.3×10^{-2}, respectively. The specimen with *H*/*D* of 2.0 is regarded as a standard; the peak stress and peak strain of the specimen with *H*/*D* of 1.5, 1.0, 0.8 and 0.6 increase by 15.64%, 35.20%, 36.66%, 96.99% and 36.84%, 84.21%, 121.05%, 178.95%, respectively. It means that the axial stress and strain negatively correlate with the *H*/*D*. However, during the post-peak failure stage, the axial strains of specimens with *H*/*D* of 2.0, 1.5, 1.0, 0.8 and 0.6 respectively increase by 3.12×10^{-3}, 1.04×10^{-3}, 1.48×10^{-3}, 1.30×10^{-3} and 0.13×10^{-3}, taking the

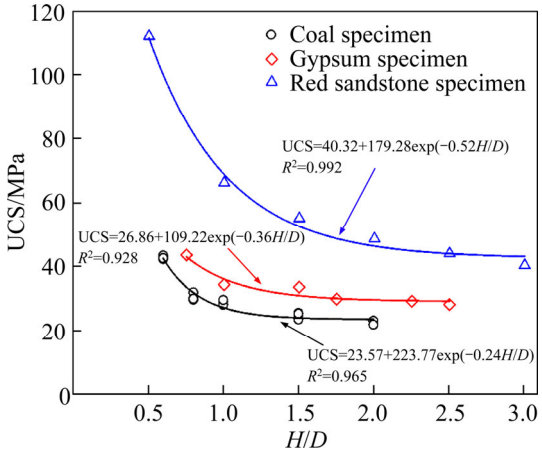

Figure 2 Fitting curves of UCS with *H*/*D* of different cylindrical specimens

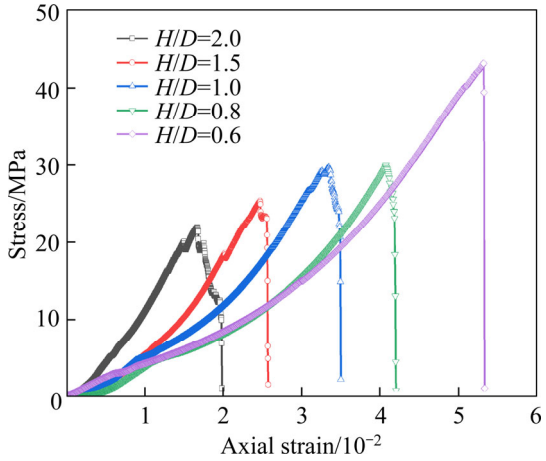

Figure 3 Axial stress−strain curves of coal specimens with different *H*/*D*s

proportion of the whole axial strain being 15.73%, 4.04%, 4.23%, 3.09% and 0.25%, respectively. In addition, the axial stress reduction rate is negatively correlated with the *H*/*D*, which means that the specimen with a smaller *H*/*D* is more prone to be damaged suddenly at the post-peak failure stage.

3.2 Acoustic emission characteristics

The principle of acoustic emission detection is that the material is deformed or damaged under the action of external action, and the acoustic signal is generated and emitted, through which the internal defects and state changes of the material can be inferred [32]. The acoustic emission monitoring of coal is helpful to understand its damage and failure characteristics. The commonly used AE parameters include AE counts, energy, amplitude, etc.

3.2.1 Evolution of AE counts

The evolution of AE counts in response to the loading time for coal specimens with different *H*/*D*s is shown in Figure 4. In the process of uniaxial compression, the AE counts at different stages are different. But for all the specimens with different *H*/*D*s, the AE counts show a similar trend at loading process and can be divided into four stages.

During OA stage, the AE counts of coal specimen with different *H*/*D*s maintain at a lower level basically except individual fluctuations, and the accumulative AE counts grow slowly, which means

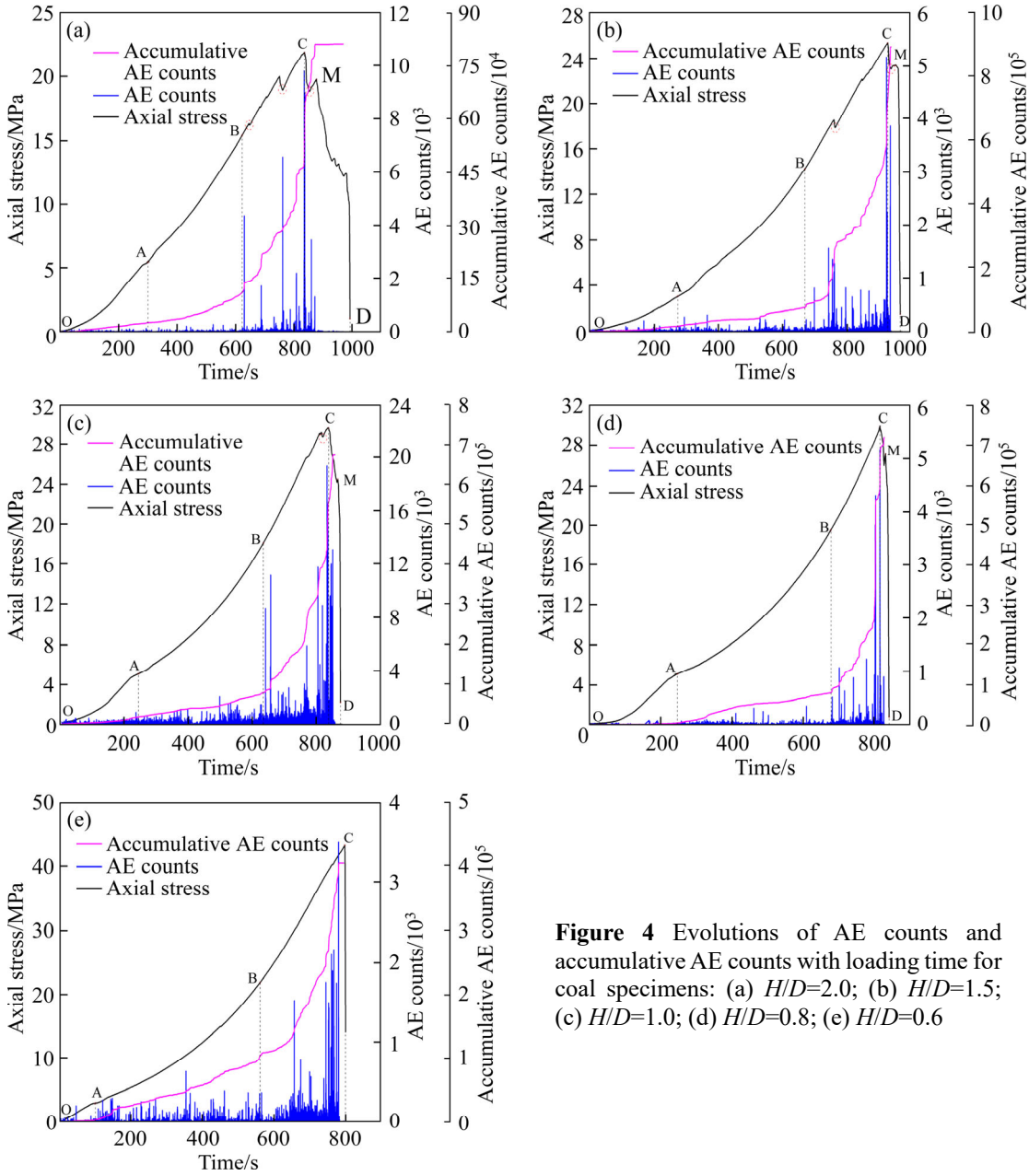

Figure 4 Evolutions of AE counts and accumulative AE counts with loading time for coal specimens: (a) *H*/*D*=2.0; (b) *H*/*D*=1.5; (c) *H*/*D*=1.0; (d) *H*/*D*=0.8; (e) *H*/*D*=0.6

that almost no AE signals occurred at this stage (as shown in Figures 4(a)−(e)). Therefore, the OA stage can be regarded as a quiet period of AE activities. The individual fluctuations were mainly attributed to the initial micro-cracks inside the coal specimens compacted. The accumulative AE counts for coal specimen with *H*/*D* of 2.0, 1.5, 1.0, 0.8, and 0.6 at this stage are 2.62×10^4, 1.65×10^4, 1.85×10^4, 0.46×10^4 and 0.44×10^4, which account for 3.20%, 1.85%, 2.75%, 0.64% and 1.08% of the total accumulative AE counts respectively. It means that the greater the *H*/*D* is, the more the initial micro-cracks inside the coal specimens contain, and the more AE signals will be released when the initial micro-cracks are compacted.

As the axial stress entered AB stage, the AE activities enhanced relatively, but they still maintained at a lower level. However, the accumulative AE counts show a near linear growth trend. Therefore, the AB stage can be considered a relatively active period of AE activities. The accumulative AE counts for coal specimen with *H*/*D* of 2.0, 1.5, 1.0, 0.8 and 0.6 at this stage are 8.40×10^4, 5.90×10^4, 6.06×10^4, 7.58×10^4 and 9.25×10^4, which account for 10.33%, 6.60%, 9.02%, 10.53%, and 22.84% of the total accumulative AE counts respectively. During this stage, the axial stress is not enough to force the coal specimen to generate new micro-cracks, but the initial micro-cracks inside coal specimens were further compacted and produced relatively more AE activities.

The AE activity of coal specimens with different *H*/*D*s became intensely during BC stage. The BC stage can be regarded as an active period of AE activities. The AE counts increased significantly, and the accumulative AE counts showed a rapid growth trend. It means that massive new cracks were produced inside coal specimens. This phenomenon is mainly attributed to the sudden slippage of the internal crack boundary inside coal specimen. Cracks interconnected and propagated, resulting in a large number of acoustic emission activities. It is worth noting that as soon as the axial stress reaches the peak stress, the peak AE count occurs and the accumulative AE counts increase sharply. At the peak stress (point C), the AE counts of the coal specimen with *H/D* of 2.0, 1.5, 1.0, 0.8 and 0.6 are 9.82×10^3, 5.17×10^3, 1.94×10^3, 5.16×10^3 and 3.50×10^3, respectively. The accumulative AE counts are 4.89×10^5, 6.68×10^5, 4.79×10^5, 6.17×10^5 and 3.00×10^5, respectively, which accounts for 60.15%, 74.66%, 71.27%, 85.64% and 74.07% of the accumulative AE counts respectively. In addition, Figures 4(a)−(e) also show that the rapidly increasing AE counts and cumulative AE counts decrease with the decrease of *H*/*D*.

During CD stage, the micro-cracks propagated and aggregated continuously to form macro-cracks, which intensified the internal damage of coal specimens. As shown in Figures 4(a)−(e), the AE signals were still produced at this stage, but the AE activities showed a decreased trend. Therefore, the CD stage can be considered a rapid decline period of AE activities. The accumulative AE counts of the coal specimens with *H*/*D* of 2.0, 1.5, 1.0, 0.8 and 0.6 at CD stage were 2.14×10^5, 1.51×10^5, 1.14×10^5, 0.23×10^5 and 0, which accounted for 26.32%, 16.89%, 16.96%, 3.19% and 0% of the total accumulative AE counts respectively. It means that the smaller the *H*/*D* is, the less the accumulative AE counts in CD stage are, and the less the proportion in total accumulative AE counts is. This is mainly attributed to the fact that the coal specimen with greater *H*/*D* has lower stress reduction rate, more micro-cracks inside of coal specimens developed and aggregated to form macro-cracks inside coal specimens while AE signals generated continuously.

3.2.2 Effect of *H*/*D* on spatial evolution of AE events

The spatial evolution of AE events is used to reflect the evolution of rock internal damage [36]. The location map of AE events reflects the location of AE events source, the initial location of crack initiation, damage characteristics and crack evolution degree of coal specimens during the loading process. The spatial evolution of AE events for the coal specimens with *H*/*D* of 2.0, 1.5, 1.0, 0.8 and 0.6 is showed in Figures 5 to 9, respectively. The blue points are the center position of AE sensors on the surface of coal specimens, and the AE event points are presented by the red dots. Table 2 shows the number of accumulative AE event points at different loading stage and their proportion to its total number of AE event points. Since the same AE signal is received by the four sensors at different times, the arrival times can be automatically obtained, analyzed, and calculated by the software (DS5 full information acoustic emission analysis software) to determine its source position.

During OA stage, the AE event points were generated randomly in the coal specimens with *H*/*D*

of 2.0, 1.5, 1.0, 0.8 and 0.6 (as shown in Figures 5(a)−(c), Figures 6(a)−(c), Figures 7(a) and (b), Figures 8(a) and (b) and Figure 9(a), respectively). This is mainly attributed to the compaction effect of the initial micro-cracks inside coal specimens under the uniaxial compression. However, the AE events of the coal specimens with *H*/*D* of 2.0, 1.5, 1.0, 0.8 and 0.6 generated at this stage account for 14.63%, 14.57%, 8.30%, 4.02% and 1.18% of their total number of AE events respectively. It means that the incidence of AE events inside coal specimens at OA stage is generally positively correlated with the *H*/*D*, and it also means that the higher the *H*/*D* is, the greater the probability of initial micro-cracks inside coal specimens will be.

With the increase of axial stress, the number of AE event points of the coal specimens with different *H*/*D*s increased slightly and began to show a gradually aggregated trend at AB stage (as shown in Figures 5(d)−(e), Figures 6(d)−(f), Figures 7(c)−(f), Figures 8(c)−(f) and Figures 9(b)−(g), respectively). This is mainly due to the fact that the initial micro-cracks were further compacted, causing slippage and misalignment between the micro-cracks,

Table 2 AE event points of coal specimen in different loading stage and their proportion to the total number

Stage	*H*/*D*=2.0		*H*/*D*=1.5		*H*/*D*=1.0		*H*/*D*=0.8		*H*/*D*=0.6	
	N	*P*/%	*N*	*P*/%	*N*	*P*/%	*N*	*P*/%	*N*	*P*/%
OA	30	14.63	36	14.57	20	8.30	14	4.02	2	1.18
AB	42	22.49	84	34.01	87	36.10	131	37.64	67	48.24
BC	120	58.54	122	49.39	113	46.89	200	57.47	101	59.41
CD	13	6.34	5	2.02	3	1.24	3	0.86	0	0
Sum	205	100	247	100	241	100	348	100	170	100

"*N*" represents the number of AE points, and "*P*" represents the proportion of the AE event points generated in different stage to the total AE event points generated in the whole experiment process.

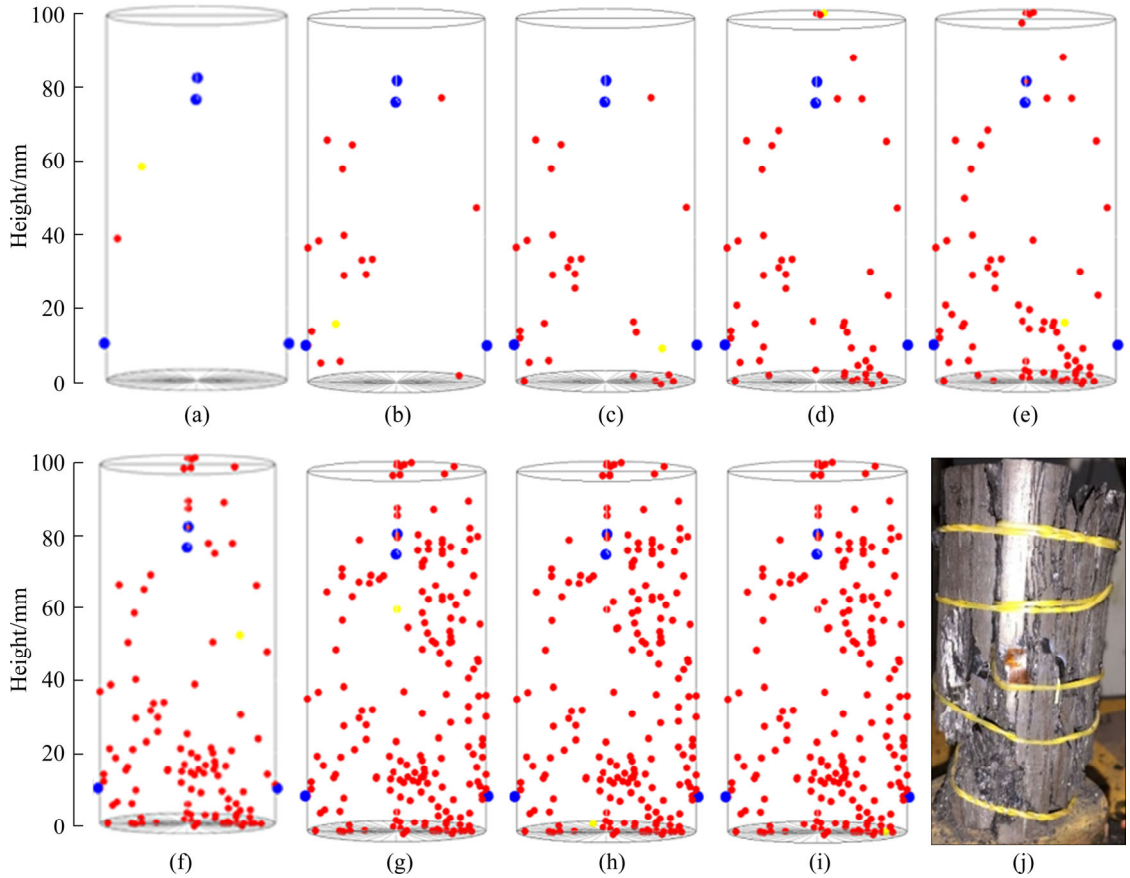

Figure 5 Spatial position of accumulative AE events in coal specimen (*H*/*D*=2.0) at different loading times: (a) 100 s; (b) 200 s; (c) 300 s; (d) 500 s; (e) 623 s; (f) 750 s; (g) 836 s; (h) 900 s; (i) 968s; (j) Failure pattern of coal specimen

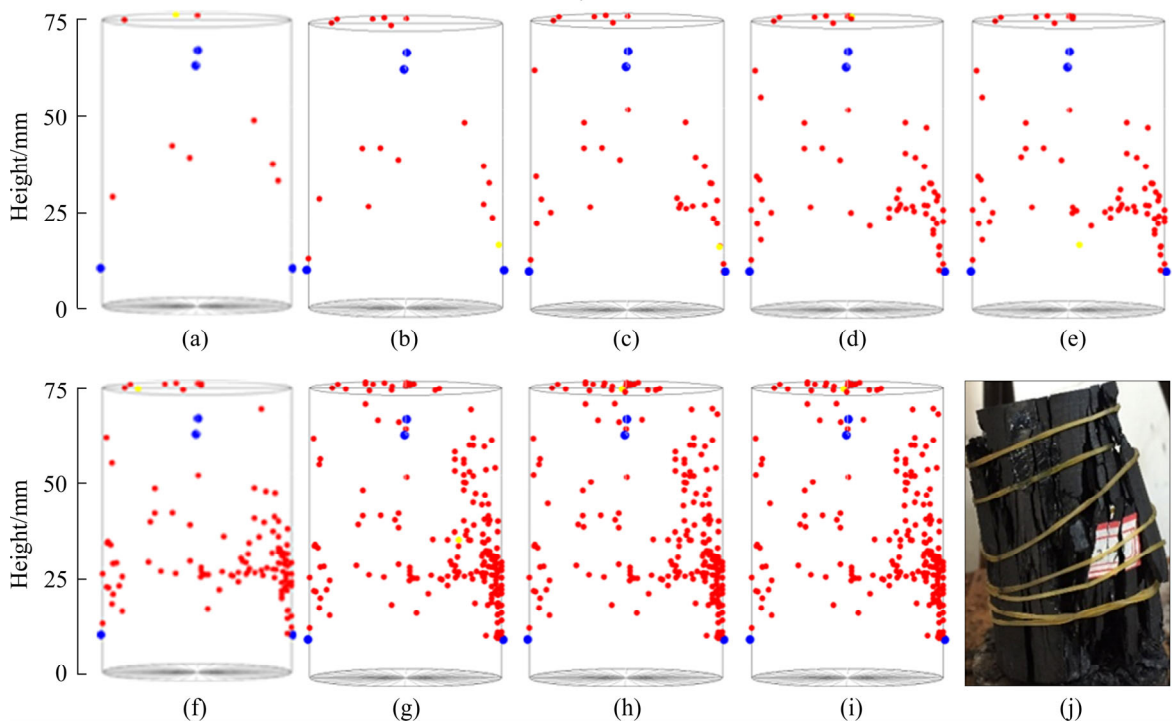

Figure 6 Spatial position of accumulative AE events in coal specimen (H/D=1.5) at different loading time: (a) 100 s; (b) 200 s; (c) 274 s; (d) 400 s; (e) 500 s; (f) 668 s; (g) 800 s; (h) 926 s; (i) 936 s; (j) Failure pattern of coal specimen

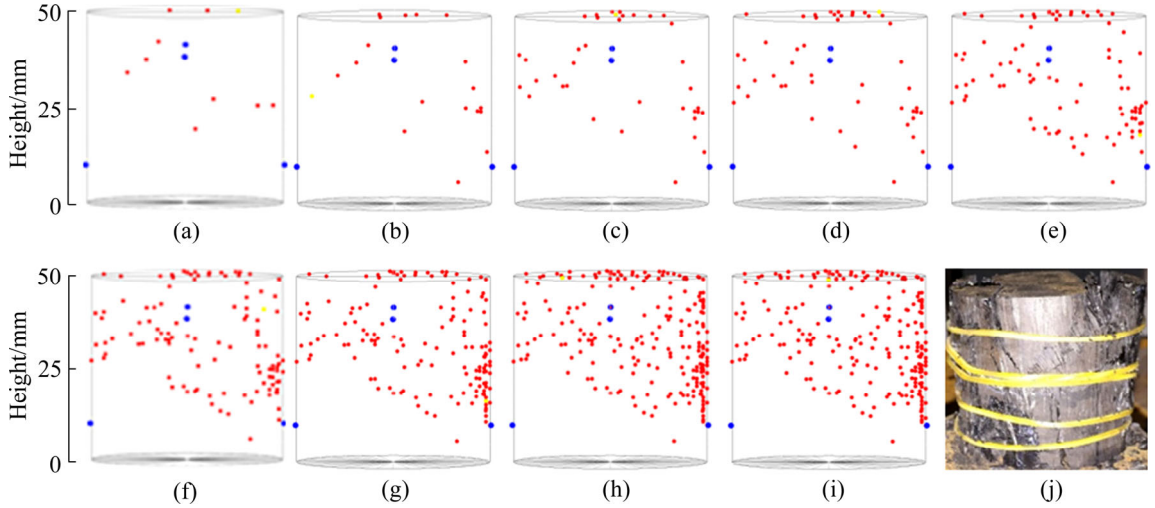

Figure 7 Spatial position of accumulative AE events in coal specimen (H/D=1.0) at different loading time: (a) 100 s; (b) 245 s; (c) 400 s; (d) 500 s; (e) 600 s; (f) 634 s; (g) 750 s; (h) 837 s; (i) 875 s; (j) Failure pattern of coal specimen

so the rough surfaces bit to each other to generate AE events. The AE events of the coal specimens with a H/D of 2.0, 1.5, 1.0, 0.8 and 0.6 generated at this stage account for 22.49%, 34.01%, 36.10%, 37.64% and 48.24% of their total number of AE events respectively.

At BC stage, the AE event points of the coal specimens with H/D of 2.0, 1.5, 1.0, 0.8 and 0.6 increased sharply, showing a further trend of aggregation, and expanding along the aggregation plane (as shown in Figures 5(f)−(g), Figures 6(g)−(h), Figures 7(g)−(h), Figures 8(g)−(j) and Figures 9(h)−(i), respectively). The deformation of coal specimens has changed from elastic deformation at AB stage to plastic deformation at BC stage. With the increase of axial stress, a large number of micro-cracks generated, expanded and aggregated continuously inside coal specimens. Therefore, a large number of AE events occurred and were recorded during this process. As shown in Table 2, the AE events of the

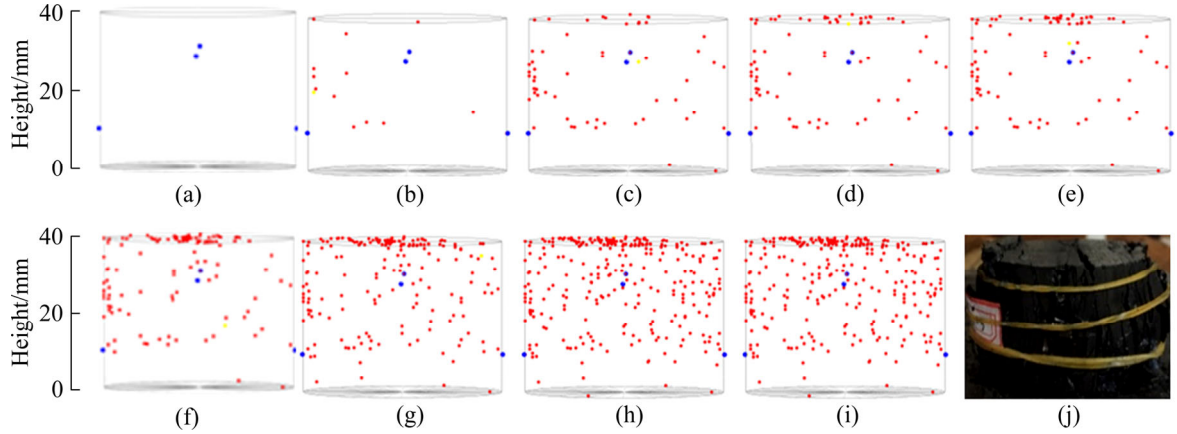

Figure 8 Spatial position of accumulative AE events in coal specimen (H/D=0.8) at different loading times: (a) 100 s; specimen (b) 246 s; (c) 350 s; (d) 400 s; (e) 500 s; (f) 677 s; (g) 750 s; (h) 818 s; (i) 841 s; (j) Failure pattern of coal

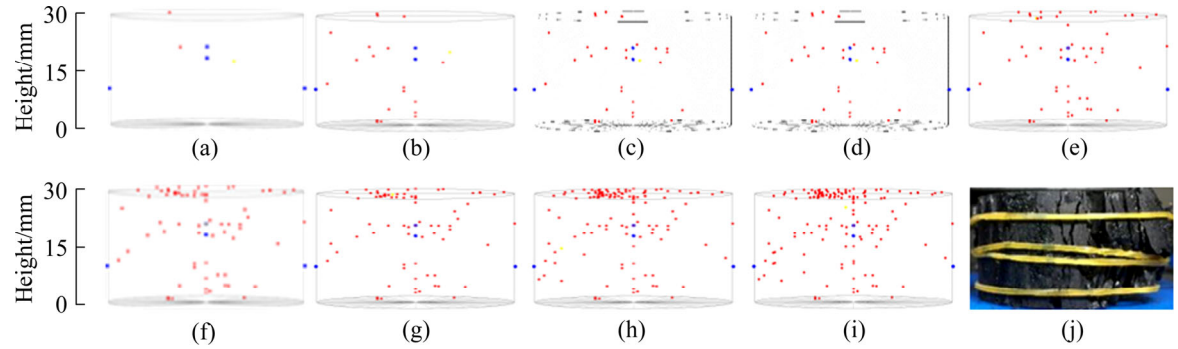

Figure 9 Spatial position of accumulative AE events in coal specimen (H/D=0.6) at different loading time: (a) 100 s; (b) 200 s; (c) 300 s; (d) 400 s; (e) 500 s; (f) 561 s; (g) 600 s; (h) 750 s; (i) 798 s; (j) Failure pattern of coal specimen

coal specimens with H/D of 2.0, 1.5, 1.0, 0.8 and 0.6 generated at this stage account for 58.54%, 49.39%, 46.89%, 57.47% and 59.41% of their total number of AE events, respectively.

The number of AE event points of coal specimens increased slightly at CD stage (as shown in Figures 5(h)−(i), Figure 6(i), Figure 7(i), Figure 8(i), and Figure 9(i) respectively). The number of AE events of the coal specimens with H/D of 2.0, 1.5, 1.0, 0.8 and 0.6 generated at this stage accounts for 6.34%, 2.02%, 1.24%, 0.86% and 0 of their total number of AE events, respectively. During this stage, the micro-cracks inside coal specimens are connected and penetrate to form the macroscopic fracture surface, which causes the loss of bearing capacity of coal specimens. However, due to the fact that the energy released by micro-cracks propagation was absorbed by newly generated micro-cracks or dissipated by the friction between the micro-crack surfaces, the strength of AE signals was weakened and many AE signals could not be recorded. Therefore, the number of recorded AE events reduced continuously. In addition, as described in Section 3.3.1, the post-peak bearing capacity of the coal specimen represented a negative correlation with the H/D. Therefore, the larger the H/D of the coal specimen is, the more the number of AE events will be generated during CD stage.

3.2.3 Effect of H/D on failure characteristic of coal specimens

The failure pattern of coal specimens under uniaxial compression is mainly related to its mechanical properties and experimental conditions [41, 42]. As shown in Figure 5(j) to Figure 9(j), the failure modes of different H/D coal samples are significantly different. Figure 5(i) to Figure 9(i) respectively show the spatial distribution characteristics of AE event points when the coal specimen with H/D of 2.0, 1.5, 1.0, 0.8 and 0.6 was destroyed. Figure 5(j) shows that a 45° shear plane appeared at the lower right part of the coal specimen when H/D was 2.0, and extended axially to the middle part and penetrated the coal specimen eventually. In addition, an axial splitting plane

appeared on the left side of the coal specimen destroyed and mainly concentrated on the upper right and lower left (as shown in Figure 5(i)). Figure 6(j) shows that several shear planes appeared on the right side of the coal specimen with *H*/*D* of 1.5. The AE event points of this coal specimen were mainly distributed on the right side and basically through the specimen (as shown in Figure 6(i)). Figure 7(j) shows that an inclined shear plane appeared on the upper left part of the coal specimen, and the upper right part was severely damaged when the *H*/*D* was 1.0. The AE event points of this coal specimen were mainly concentrated on the upper and middle right sides (as shown in Figure 7(i)). Different from the above, when *H*/*D* is 0.8 and 0.6, many splitting planes along the axial direction appear on the coal sample, and the coal sample is seriously damaged, as shown in Figures 8(j) and 9(j). The AE event points of these two kinds of *H*/*D* coal specimens were scattered randomly throughout the coal samples (as shown in Figures 8(i) and 9(i)). In summary, the failure pattern of coal specimens with *H*/*D* of 2.0, 1.5 and 1.0 was mainly shear failure. However, the failure pattern of coal specimens with *H*/*D* of 0.8 and 0.6 was mainly splitting failure along the axial direction. Based on the comparison of Figure 5(i) to Figure 9(i) and Figure 5(j) to Figure 9(j), it can be seen that the distribution characteristics of AE event points correspond well to the failure pattern of coal specimens under uniaxial compression. Therefore, the AE event points can be used to infer the failure pattern of coal specimens.

4 Conclusions

1) The UCS and axial strain of coal specimens decrease with the *H*/*D* increasing. An empirical equation relating *H*/*D* with UCS of coal specimen is proposed based on the experimental data, and certified suitable for different rock types based on the experimental data obtained by other researchers.

2) The stress−time curve can be divided into four periods according to the variation of AE counts in response to the coal specimen deformation: quiet period, relatively active period, active period and rapid decline period. The span of quiet period and rapid decline period shorten with the *H*/*D* decreasing, and the accumulative AE counts during the quiet period and rapid decline period also reduce with the *H*/*D* decreasing. At the active period, AE signals are recorded due to the micro-cracks expanding, evolving and merging, which can be regarded as the precursor information for predicting the instability of coal pillar. In addition, the cumulative AE counts of coal specimens showed a "slow-linear-accelerated growth" change pattern, showing a decreasing trend with the *H*/*D* increasing.

3) The real-time spatial evolution of AE event points can reflect the initiation, expansion, aggregation and connection of micro-cracks inside the coal specimen with different *H*/*D*s. The spatial distribution of AE event points corresponds well to the failure pattern of coal specimens. The shear failure was dominant of the coal specimens with *H*/*D* of 2.0, 1.5 and 1.0, and the failure pattern mainly was splitting failure along the axial direction when the *H*/*D* was 0.8 and 0.6. This study provides an important reference for predicting the instability of residual coal pillars with different *H*/*D*s by AE technology method.

Contributors

The overarching research goals were developed by GUO Yu-xia, FENG Guo-rui and ZHAO Yong-hui. ZHAO Yong-hui and GUO Yu-xia did experiment and analyzed the experimental data. The initial draft of the manuscript was written by GUO Yu-xia and ZHAO Yong-hui. WANG Sheng-wei, ZHANG yu-jiang, FENG guo-rui, RAN Hong-yu revised the original manuscript. All the authors replied to the reviewers' comments and revised the final version.

Conflict of interest

GUO Yu-xia, ZHAO Yong-hui, WANG Sheng-wei, ZHANG yu-jiang, FENG Guo-rui and RAN Hong-yu declare that they have no conflict of interest.

References

[1] KARACAN C O, WARWICK P D. Assessment of coal mine methane (CMM) and abandoned mine methane (AMM) resource potential of longwall mine panels: Example from Northern Appalachian Basin, USA [J]. International Journal of Coal Geology, 2019, 208: 37−53. DOI: 10.1016/j.coal.2019.04.005.

[2] POULSEN B A, SHEN B, WILLIAMS D J, HUDDLESTONE-HOLMES C, ERARSLAN N, QIN J. Strength reduction on saturation of coal and coal measures

rocks with implications for coal pillar strength [J]. International Journal of Rock Mechanics and Mining Sciences, 2014, 71: 41−52. DOI: 10.1016/j.ijrmms.2014.06.012.

[3] ZHANG Yu-jiang, FENG guo-rui, ZHANG Min, REN Hong-rui, BAI Jin-wen, GUO Yu-xia, JIANG Hai-na, KANG Li-xun. Residual coal exploitation and its impact on sustainable development of the coal industry in China [J]. Energy Policy, 2016, 96: 534−541. DOI: 10.1016/j.enpol.2016.06.033.

[4] ISIAKA A I, DURRHEIM R J, MANZI M S D. High-resolution seismic reflection investigation of subsidence and sinkholes at an abandoned coal mine site in south africa [J]. Pure and Applied Geophysics, 2019, 176(4): 1531−1548. DOI: 10.1007/s00024-018-2026-3.

[5] FENG Guo-rui, WANG Peng-fei, CHUGH Y P. Stability of gate roads next to an irregular yield pillar: A case study [J]. Rock Mechanics and Rock Engineering, 2019, 52(8): 2741−2760. DOI: 10.1007/s00603-018-1533-y.

[6] BAI Jin-wen, FENG Guo-rui, WANG Ze-hua, WANG Shang-yong, QI Ting-ye, WANG Peng-fei. Experimental investigations on the progressive failure characteristics of a sandwiched coal-rock system under uniaxial compression [J]. Applied Sciences, 2019, 9(6): 1195. DOI: 10.3390/app9061195.

[7] HAUQUIN T, GUNZBURGER Y, DECK O. Predicting pillar burst by an explicit modelling of kinetic energy [J]. International Journal of Rock Mechanics and Mining Sciences, 2018, 107: 159−171. DOI: 10.1016/j.ijrmms.2018.05.004.

[8] WANG Fang-tian, TU Shi-hao, LI Zhao-xin, TU Hong-sheng, CHEN Fang. Mutation instability mechanism of the room mining residual pillars in the shallow depth seam [J]. Journal of Mining & Safety Engineering, 2012, 29(6): 770−775. DOI: CNKI:SUN:KSYL.0.2012-06-003. (in Chinese)

[9] ZHU Wei-bing, CHEN Lu, ZHOU Zi-long, SHEN Bao-tang, XU Yu. Failure propagation of pillars and roof in a room and pillar mine induced by longwall mining in the lower seam [J]. Rock Mechanics and Rock Engineering, 2019, 52(4): 1193−1209. DOI: 10.1007/s00603-018-1630-y.

[10] WANG Qi, GAO Hong-ke, JIANG Bei, LI Shu-cai, HE Man-chao, QIN Qian. In-situ test and bolt-grouting design evaluation method of underground engineering based on digital drilling [J]. International Journal of Rock Mechanics and Mining Sciences, 2021, 138: 104575. DOI: 10.1016/j.ijrmms.2020.104575.

[11] DAS M N. Influence of width/height ratio on post-failure behaviour of coal [J]. International Journal of Mining and Geological Engineering, 1986, 4(1): 79−87. DOI: 10.1007/BF01553759.

[12] OZKAN I, OZARSLAN A, GENIS M, OZSEN H. Assessment of scale effects on uniaxial compressive strength in rock salt [J]. Environmental and Engineering Geoscience, 2009, 15(2): 91−100. DOI: 10.2113/gseegeosci.15.2.91.

[13] QI Cheng-zhi, WANG Ming-yang, BAI Ji-ping, LI Kai-rui. Mechanism underlying dynamic size effect on rock mass strength [J]. International Journal of Impact Engineering, 2014, 68: 1−7. DOI: 10.1016/j.ijimpeng.2014.01.005.

[14] HE Gui-cheng, LI Yu-lan, DING De-xin. Experimental investigation on strength and size effect of the gypsum sample in different height to diameter ratios [J]. Chinese Journal of Underground Space and Engineering, 2016, 12(6): 1464−1470. DOI: CNKI:SUN:BASE.0.2016-06-006. (in Chinese)

[15] STAVROU A, MURPHY W. Quantifying the effects of scale and heterogeneity on the confined strength of micro-defected rocks [J]. International Journal of Rock Mechanics and Mining Sciences, 2018, 102: 131−143. DOI: 10.1016/j.ijrmms.2018.01.019.

[16] ZHANG Qi, ZHU He-hua, ZHANG Lian-yang, DING Xiao-bin. Study of scale effect on intact rock strength using particle flow modeling [J]. International Journal of Rock Mechanics and Mining Sciences, 2011, 48(8): 1320−1328. DOI: 10.1016/j.ijrmms.2011.09.016.

[17] POULSEN B A, ADHIKARY D P. A numerical study of the scale effect in coal strength [J]. International Journal of Rock Mechanics and Mining Sciences, 2013, 63: 62−71. DOI: 10.1016/j.ijrmms.2013.06.006.

[18] BAHRANI N, KAISER P K. Numerical investigation of the influence of specimen size on the unconfined strength of defected rocks [J]. Computers and Geotechnics, 2016, 77: 56−67. DOI: 10.1016/j.compgeo.2016.04.004.

[19] WANG Y, FENG W K, HU R L, LI C H. Fracture evolution and energy characteristics during marble failure under triaxial fatigue cyclic and confining pressure unloading (FC-CPU) conditions [J]. Rock Mechanics and Rock Engineering, 2021, 54: 799−818. DOI: 10.1007/s00603-020-02299-6.

[20] MA Xiao-dong. Volumetric deformation, ultrasonic velocities and effective stress coefficients of St Peter sandstone during poroelastic stress changes [J]. Rock Mechanics and Rock Engineering, 2019, 52(9): 2901−2916. DOI: 10.1007/s00603-019-01750-7.

[21] KONG Xiang-guo, WANG En-yuan, HE Xue-qiu, ZHAO En-lai, ZHAO Chuan. Mechanical characteristics and dynamic damage evolution mechanism of coal samples in compressive loading experiments [J]. Engineering Fracture Mechanics, 2019, 210: 160−169. DOI: 10.1016/j.engfracmech.2018.04.005.

[22] LIU Xiao-ming, WU Shao-peng, YANG Xiao-li. Smart characteristics of conductive asphalt concrete [J]. Journal of Central South University of Technology (Science and Technology), 2009, 40(5): 1465−1470. DOI: JournalArticle/5af4a7fec095d718d81c3c00. (in Chinese)

[23] YANG Yong-liang, ZHENG Kai-yue, LI Zhi-wei, LI Zeng-hua, SI Lei-lei, HOU Shi-song, DUAN Yu-jian. Experimental study on pore-fracture evolution law in the thermal damage process of coal [J]. International Journal of Rock Mechanics and Mining Sciences, 2019, 116: 13−24. DOI: 10.1016/j.ijrmms.2019.03.004.

[24] HAN Peng-ju, WANG Shuai, CHEN You-jia, BAI Xiao-hong. Mechanism of cement-stabilized soil polluted by magnesium sulfate [J]. Journal of Central South University, 2015, 22(5): 1869−1877. DOI: 10.1007/s11771-015-2706-4.

[25] ZHU Zhen-de, NI Xiao-hui, WANG Wei, LI Shuang-bei, ZHAO Jie, WU Yi-quan. Dynamic experimental study on rock

meso-cracks growth by digital image processing technique [J]. Journal of Central South University of Technology, 2008, 15(S2): 114−120. DOI: 10.1007/s11771-008-0445-5.

[26] XIAO Jia, WANG Jian-hua, CHEN Lei, ZHAO Jin-hui. Damage mechanism of cement-ground limestone cementitious material under sulfate attack condition [J]. Journal of Central South University of Technology (Science and Technology), 2009, 40(1): 230−235. DOI: CNKI: SUN:ZNGD.0.2009-01-042. (in Chinese)

[27] DU Xian-jie, FENG Guo-rui, QI Ting-ye, GUO Yu-xia, ZHANG Yu-jiang, WANG Ze-hua. Failure characteristics of large unconfined cemented gangue backfill structure in partial backfill mining [J]. Construction and Building Materials, 2018, 194: 257−265. DOI: 10.1016/j.conbuildmat.2018.11.038.

[28] XIAO Peng, LI Di-yuan, ZHAO Guo-yan, ZHU Quan-qi, LIU Huan-xin, ZHANG Chun-shun. Mechanical properties and failure behavior of rock with different flaw inclinations under coupled static and dynamic loads. [J]. Journal of Central South University, 2020, 27(10): 2945−2958. DOI: 10.1007/s11771-020-4520-x.

[29] ZHAO Guo-yan, WANG En-jie, WU Hao, QIU Ju, DAI Yi-wen. Micro-fracture evolution rule of sandstone specimens with a single hole under uniaxial compression [J]. Journal of Central South University of Technology (Science and Technology), 2019, 50(8): 1891−1900. DOI: CNKI:SUN: ZNGD.0.2019-08-017. (in Chinese)

[30] LI De-xing, WANG En-yuan, KONG Xiang-guo, ZHAO Shuai, KONG Yan-hui, WANG Xiao-ran, WANG Dong-ming, LIU Quan-lin. Mechanical properties and electromagnetic radiation characteristics of concrete specimens after exposed to elevated temperatures [J]. Construction and Building Materials, 2018, 188: 381−390. DOI: 10.1016/j.conbuildmat.2018.07.236.

[31] WAN Guo-xiang, LI Xi-bing, WANG Qi-sheng. Effect of linear joint on propagation of rock electromagnetic emission [J]. Journal of Central South University (Science and Technology), 2011, 42(4): 1133−1139. DOI: CNKI:SUN: ZNGD.0.2011-04-045. (in Chinese)

[32] YANG Wei-min, GENG Yang, ZHOU Zong-qing, LI Lian-chong, DING Ruo-song, WU Zhong-hu, ZHAI Ming-yang. True triaxial hydraulic fracturing test and numerical simulation of limestone [J]. Journal of Central South University, 2020, 27(10): 3025−3039. DOI: 10.1007/s11771-020-4526-4.

[33] CHU Chao-qun, WU Shun-chuan, ZHANG Shi-huai, GUO Pei, ZHANG Min. Mechaincal behavior anisotropy and fracture characteristics of bedded sandstone [J]. Journal of Central South University (Science and Technology), 2020, 51(8): 2232−2246. DOI: CNKI:SUN:ZNGD.0.2020-08-018. (in Chinese)

[34] CHEN Xu, TANG Chun-an, YU Jin, ZHOU Jian-feng, CAI Yan-yan. Experimental investigation on deformation characteristics and permeability evolution of rock under confining pressure unloading conditions [J]. Journal of Central South University, 2018, 25(8): 1987−2001. DOI: 10.1007/s11771-018-3889-2.

[35] YANG Hui-ming, WEN Guang-cai, HU Qian-ting, LI Yuan-yuan, DAI Lin-chao. Experimental investigation on influence factors of acoustic emission activity in coal failure process [J]. Energies, 2018, 11(6): 1414. DOI: 10.3390/en11061414.

[36] ZHANG Shi-hua, WU Shun-chuan, CHU Chao-yun, GUO Pei, ZHANG Guang. Acoustic emission associated with self-sustaining failure in low-porosity sandstone under uniaxial compression [J]. Rock Mechanics and Rock Engineering, 2019, 52(7): 2067−2085. DOI: 10.1007/s00603-018-1686-8.

[37] SHKURATNIK V L, FILIMONOV Y L, KUCHURIN S V. Experimental investigations into acoustic emission in coal samples under uniaxial loading [J]. Journal of Mining Science, 2004, 40(5): 458−464. DOI: 10.1007/s10913-005-0030-3.

[38] LI De-xing, WANG En-yuan, KONG Xiang-guo, ALI M, WANG Dong-ming. Mechanical behaviors and acoustic emission fractal characteristics of coal specimens with a pre-existing flaw of various inclinations under uniaxial compression [J]. International Journal of Rock Mechanics and Mining Sciences, 2019, 116: 38−51. DOI: 10.1016/j.ijrmms.2019.03.022.

[39] ULUSAY R. The ISRM suggested methods for rock characterization, testing and monitoring: 2007-2014 [M]// Springer International Publishing, 2015, 74(4): 47−48. DOI: 10.1007/s10064-015-0780-3.

[40] LIU Gang, XIAO Fu-kun, QIN Tao. Rock mechanics characteristics and acoustic emission rule under small-size effect [J]. Chinese Journal of Rock Mechanics and Engineering, 2018, 37(S2): 3905−3917. DOI: CNKI:SUN: YSLX.0.2018-S2-012. (in Chinese)

[41] MENG Qing-bin, HAN Li-jun, PU Hai, LI Hao, WEN Sheng-yong. Effect of the size and strain rate on the mechanical behavior of rock specimens [J]. Journal of China University of Mining & Technology, 2016, 45(2): 233−243. DOI: CNKI:SUN:ZGKD.0.2016-02-006. (in Chinese)

[42] YANG Sheng-qi, SU Cheng-dong, XU Wei-ya. Experimental and theoretical study of size effect of rock material [J]. Engineering Mechanics, 2005, 22(4): 112−118. DOI: 10.3969/j.issn.1000-4750.2005.04.022. (in Chinese)

(Edited by YANG Hua)

中文导读

不同高径比煤岩单轴压缩破坏过程的应力-应变-声发射响应

摘要：遗留煤柱在相邻煤层安全开采、采空区管理和维护废弃矿井稳定性等方面发挥着重要作用。高径比影响着遗留煤柱的稳定性。本文对 5 种高径比(2.0，1.5，1.0，0.8 和 0.6)的煤样进行了单轴压缩试验，并对应力、应变和声发射进行了监测。结果表明，随着高径比的减小，煤样的单轴抗压强度和峰值应变均增大。提出了一个用以描述单轴抗压强度和高径比关系的经验方程。煤样破坏过程中的声发射活动可被划分为四个时期，静默期和快速衰弱期的时长与高径比呈正相关。高径比越小，煤样的破坏特征越复杂，当高径比为 2.0，1.5，1.0 时，破坏形式以剪切破坏为主，而当高径比为 0.8，0.6 时，破坏形式以轴向劈裂破坏为主。声发射事件点的实时空间演化可以反映微裂隙的萌生、扩展、聚集和联通。

关键词：遗留煤柱；高径比；单轴压缩；声发射；微裂隙演化